Journal of Membrane Science 383 (2011) 289–300

Contents lists available at SciVerse ScienceDirect

Journal of Membrane Science

journal homepage: www.elsevier.com/locate/memsci

Maxwell–Stefan modeling of slowing-down effects in mixed gas permeation across porous membranes

Rajamani Krishna*, Jasper M. van Baten

Van 't Hoff Institute for Molecular Sciences, University of Amsterdam, Science Park 904, 1098 XH Amsterdam, The Netherlands

ARTICLE INFO

Article history:
Received 18 July 2011
Received in revised form 24 August 2011
Accepted 30 August 2011
Available online 3 September 2011

Keywords:
Permeation selectivity
Correlation effects
Adsorption
Maxwell–Stefan diffusion
CO_2 capture

ABSTRACT

Micro- and meso-porous materials such as zeolites, metal-organic frameworks (MOFs), covalent-organic frameworks (COFs), zeolitic imidazolate frameworks (ZIFs), Vycor glass, MCM-41, and SBA-15 are used in membrane separation in a wide variety of applications such as CO_2 capture. For process development and design purposes the Maxwell–Stefan (M–S) equations are widely used for modeling mixed gas permeation. In the M–S formulation we have basically two types of diffusivities: (a) $Đ_i$, that characterize species i–wall interactions in the broadest sense and (b) exchange coefficients $Đ_{ij}$ that reflect how the facility for transport of species i *correlates* with that of species j. Such correlations have the effect of slowing-down the more mobile partner species in the mixtures. In many cases the $Đ_i$ corresponds to the value of the pure component i; consequently these can be estimated from unary permeation data. The $Đ_{ij}$, on the other hand are not directly accessible from experimental data. The major objective of this communication is to stress the importance of proper estimation of the exchange coefficients $Đ_{ij}$. To achieve this objective, and to illustrate the variety of issues involved, we consider permeation of CO_2/H_2, CO_2/N_2, CO_2/CH_4, and CH_4/H_2 mixtures across membranes with crystalline layers of four different materials: MFI (intersecting channels of 5.5 Å size), BTP-COF (one-dimensional hexagonal-shaped channels of 34 Å), LTA-Si zeolite (11.2 Å cages separated by 4.11 Å × 4.47 Å sized windows), and MgMOF-74 (1D hexagonal-shaped channels of 10.4 Å size). The required data on pure component adsorption isotherms are obtained from configurational-bias Monte Carlo (CBMC) simulations. The M–S diffusivities are determined from molecular dynamics (MD) simulations.

Our studies show that the permeation selectivities are crucially dependent on the proper modeling of the correlation effects. Increased upstream feed pressures lead to significant enhancement in permeation selectivities; this enhancement is directly traceable to the increase of the correlation effects with increased loadings. Use of some commonly used approaches, suggested in the published literature, lead to severe underestimation of permeation selectivities.

1. Introduction

A wide variety of *micro*- and *meso*-porous materials are of potential use in separation applications, such as CO_2 capture [1–11]. Examples of *micro*-porous materials include zeolites (crystalline aluminosilicates), metal-organic frameworks (MOFs), covalent-organic frameworks (COFs), zeolitic imidazolate frameworks (ZIFs), carbon nanotubes (CNTs), carbon molecular sieves (CMS), and titanosilicates (such as ETS-4, and ETS-10). Examples of *meso*-porous materials include SBA-16, MCM-41, and Vycor glass. In the case of mixed matrix membranes, zeolites, MOFs, ZIFs, or CNTs are embedded within a polymer or silica matrix [12–15].

For the development of membrane separation technologies, there is a need for proper modeling of mixture permeation across the chosen membrane material. The appropriate models to describe mixture permeation must take proper account of the influence each of the diffusing species exerts on its partner molecules. Generally speaking, the tardier species has a retarding influence on the more mobile species. For illustration purposes consider the experimental data of Sandström et al. [16] for permeances of CO_2 and H_2 across an MFI zeolite membrane of 0.7 μm thickness. MFI zeolite consists of a set of intersecting channels of approximately 5.5 Å in size. Fig. 1a presents a comparison of the permeances of CO_2 and H_2 for CO_2/H_2 mixture permeation with the corresponding data on unary permeances. We note that the permeance of the tardier CO_2 in the mixture is practically the same as that for unary diffusion for the entire range of upstream (feed) partial pressures. For H_2, the permeance in the mixture is about an order of magnitude lower than for unary diffusion. Furthermore, we note that the H_2 permeance in

* Corresponding author. Tel.: +31 20 6270990; fax: +31 20 5255604.
E-mail address: r.krishna@uva.nl (R. Krishna).

0376-7388/$ – see front matter © 2011 Elsevier B.V. All rights reserved.
doi:10.1016/j.memsci.2011.08.067

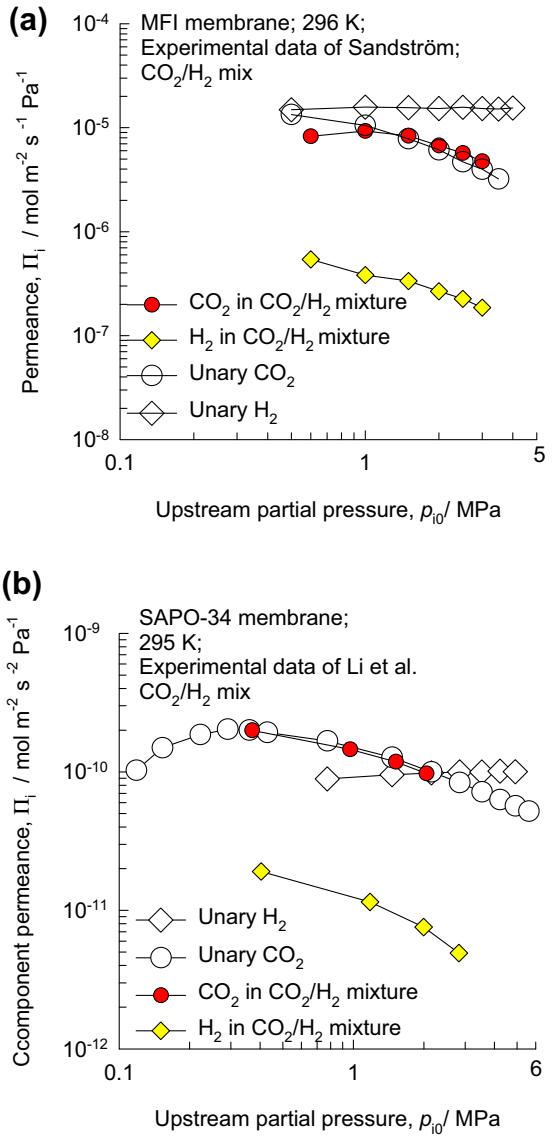

Fig. 1. Comparison of the permeances of CO_2 and H_2 for CO_2/H_2 mixture permeation with data on unary permeances for (a) MFI and (b) SAPO-34 membranes. The MFI permeation data are from Sandström et al. [16]. The SAPO-34 permeation data are from Li et al. [17–19].

the mixture is progressively reduced as the upstream (feed) pressure is increased. Sandström et al. [16] consider the reduction in the H_2 permeance to be a result of "blocking" by the partner CO_2 molecules.

An exactly analogous situation occurs for CO_2/H_2 mixture permeation across a SAPO-34 membrane; SAPO-34 consists of 8.5 Å size cages separated by 3.8 Å × 4.2 Å size windows. Fig. 1b presents the data from experiments data of Li et al. [17–19]. We note that the permeance of CO_2 in the mixture is practically identical to that for unary diffusion. In sharp contrast, the permeance of H_2 in the mixture is about an order of magnitude lower than for pure H_2 diffusion. As in the case of MFI membrane, the permeance of H_2 in the mixture falls progressively below that for unary diffusion as the upstream feed pressure is increased.

Slowing-down effects are the root cause of the decrease in the H_2/CO_2 selectivity of Matrimid membrane with increasing proportion of CO_2 in the CO_2/H_2 mixture in the upstream (feed) compartment [20]. Blocking, slowing-down, or "hindering" effects also manifest for mixtures other than CO_2/H_2, and appear to be a generic characteristic of mixture permeation across a variety of porous membrane materials [19–27]. For water–alcohol and alcohol–acetone mixtures, there is mutual slowing-down of each of the components due to hydrogen bonding effects [28–33].

For modeling n-component mixture permeation inside either micro- or meso-porous membranes, it is commonly accepted that the fundamentally correct approach is to relate the fluxes N_i, defined in terms of the cross-sectional area of the membrane, to the chemical potential gradients $\nabla\mu_i$ by use of the Maxwell–Stefan (M–S) equations [17,26,34–37]:

$$-\phi\frac{c_i}{RT}\frac{d\mu_i}{dz} = \sum_{\substack{j=1\\ j\neq i}}^{n}\frac{x_jN_i - x_iN_j}{Đ_{ij}} + \frac{N_i}{Đ_i}; \quad i = 1, 2, \ldots n \tag{1}$$

where ϕ represents the fractional pore volume of the porous material, and the concentrations c_i are defined in terms of moles per m^3 of accessible pore volume. The x_i in Eq. (1) is the component mole fractions of the adsorbed phase within the micropores:

$$x_i = \frac{c_i}{c_t}; \quad i = 1, 2, \ldots n \tag{2}$$

The $Đ_i$ characterize species i–wall interactions in the broadest sense. In many cases the $Đ_i$ corresponds to the value of the pure component i; consequently this can be estimated from unary permeation data. In some cases where molecular clustering occurs, the $Đ_i$ in the mixture can be lower than that of pure components [30,31]. The $Đ_{ij}$ are exchange coefficients representing interaction between components i with component j. At the molecular level, the $Đ_{ij}$ reflect how the facility for transport of species i *correlates* with that of species j. Conformity with the Onsager reciprocal relations prescribes:

$$Đ_{ij} = Đ_{ji} \tag{3}$$

In the M–S formulation (1), the exchange coefficients $Đ_{ij}$ account for slowing-down effects. In order to illustrate this, Fig. 2 presents MD simulation data for the M–S diffusivities, $Đ_1$, $Đ_2$, and $Đ_{12}$ for diffusion of equimolar ($c_1 = c_2$) CO_2 (1)/H_2 (2) mixtures at 300 K in four different materials: (a) MFI zeolite, (b) all-silica LTA-Si (11.2 Å cages separated by 4.11 Å × 4.47 Å sized windows), (c) MgMOF-74 (1D hexagonal-shaped channels of 10.4 Å size [8,9,37,38]), and (d) BTP-COF (1D hexagonal-shaped channels of 34 Å size [39]). The MD simulation methodology is described in Supplementary Material accompanying this publication. In the limit of low concentrations, say $c_t < 1$ kmol m^{-3}, we have $Đ_{12} \gg Đ_2 > Đ_1$. Consequently, the contribution of the first right member of Eq. (1) can be considered to be negligible, and the permeation fluxes at very low loadings will correspond to that for unary permeation. For all topologies the exchange coefficient $Đ_{12}$ shows a significant reduction in magnitude with increasing pore concentration; consequently correlation effects increase with increasing pore concentrations. For all four pore topologies, the M–S diffusivity of CO_2, $Đ_1$, is significantly lower than the binary exchange coefficient $Đ_{12}$. Consequently, the influence of the first right member of Eq. (1) on the flux of CO_2 is relatively small, i.e. coupling effects are not expected to have a significant effect on CO_2 permeation flux in the mixture. This is the reason that the permeance of CO_2 in the mixture is practically the same as for pure components (cf. Fig. 1).

The situation with regard to H_2 is completely different. With increased pore concentrations c_t, the binary exchange coefficient $Đ_{12}$ is lowered to values below that of the M–S diffusivity of H_2, $Đ_2$. Consequently, the influence of the first right member of Eq. (1) on the flux of H_2 is non-negligible. This is the reason that the permeance of H_2 in the mixture is progressively lower than that for the pure component (cf. Fig. 1).

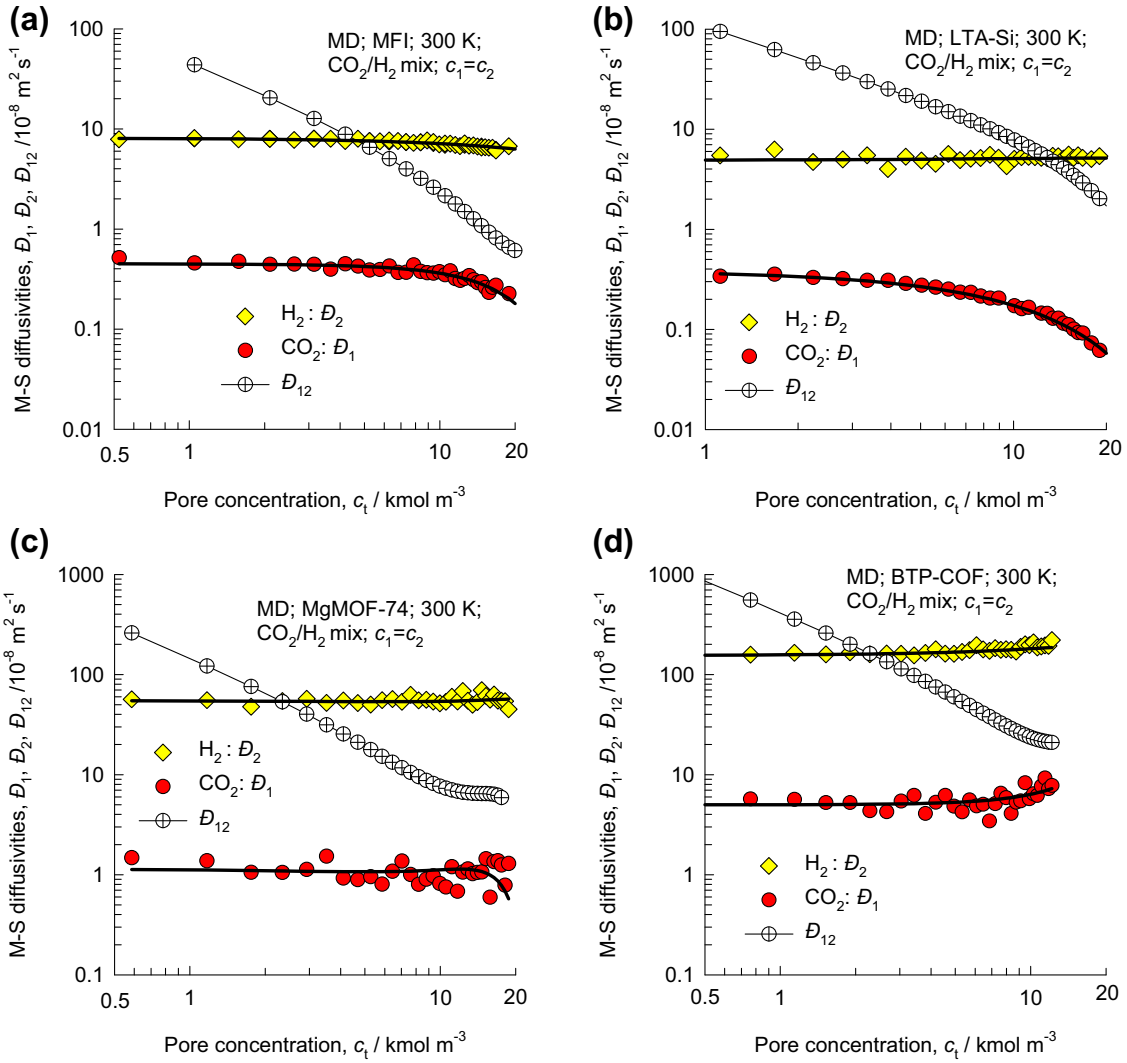

Fig. 2. The Maxwell–Stefan diffusivities, $Đ_1$, $Đ_2$, and $Đ_{12}$ for diffusion of equimolar ($c_1 = c_2$) $CO_2(1)/H_2(2)$ mixtures at 300 K in (a) MFI, (b) LTA-Si, (c) MgMOF-74, and (d) BTP-COF as a function of the total concentration, c_t. The M–S diffusivities $Đ_1$, and $Đ_2$ are from unary MD simulations. The concentration dependence of the M–S diffusivities are described using the Reed and Ehrlich model [23,36,53], using the parameters specified in Supplementary material. The binary exchange coefficient $Đ_{12}$ is determined from mixture MD simulations, using the methodology described in Supplementary material, which also contains analogous data comparisons for $Đ_1$, $Đ_2$, and $Đ_{12}$ for a much wider variety of guest/host combinations.

The key to the accurate modeling of mixture permeation lies in the proper estimation of the exchange coefficients $Đ_{12}$, especially its concentration dependence. This is a challenging task because there is no direct experimental procedure for its estimation from membrane permeation data. PFG NMR experimental studies on the self-diffusivities in mixtures [40] give an indication of the mutual influence of one adsorbed species on its partner molecules; these experiments do not yield information on the exchange coefficients $Đ_{12}$. The major objectives of the present communication are: (1) to use MD simulations for providing insights into the magnitude of $Đ_{12}$ in a variety of porous materials of practical importance, (2) to suggest practical procedures for estimation of $Đ_{12}$, and (3) to point out pitfalls in some procedures suggested in the published literature for estimation of $Đ_{12}$.

Supplementary material accompanying this publication gives information on the specific force fields used, unit cell dimensions, accessible pore volume, characteristic pore dimensions, molecular simulation methodologies, pore landscapes and snapshots, along with the entire database of simulation data on isotherms, heats of adsorption, and diffusivities. Besides BTP-COF, MgMOF-74, LTA-Si, and MFI, adsorption and diffusion data for a variety of other host materials (CHA, FAU-Si, NaY, NaX, IRMOF-1, and MOF-177) are also presented in Supplementary material in order to stress the generic nature of the conclusions drawn in this work.

2. Estimation of the Maxwell–Stefan exchange coefficients $Đ_{12}$

An important advantage of formulating the M–S equations (1) in terms of concentration c_i within the pores is that the exchange coefficient $Đ_{12}$ are relatable to the corresponding M–S diffusivity in the binary *fluid* mixture, with species 1 and 2. This is illustrated in Fig. 3 which presents data on $Đ_{12}$, as a function of the total concentration, c_t, for six different binary mixtures in a variety of other host materials. In mesoporous BTP-COF, the values of the exchange coefficient $Đ_{12}$ are the nearly the same as the binary *fluid phase* M–S diffusivity, $Đ_{12,fl}$, over the entire range of pore concentrations. A similar result holds for mesopores in the 20–100 Å size range [35].

For micro-porous materials, the $Đ_{12}$ are lower than the corresponding fluid phase diffusivity $Đ_{12,fl}$ by a factor, F, that depends on the degree of confinement within the micropores. The stronger the degree of confinement, the smaller is the value of F [35,36]. Within

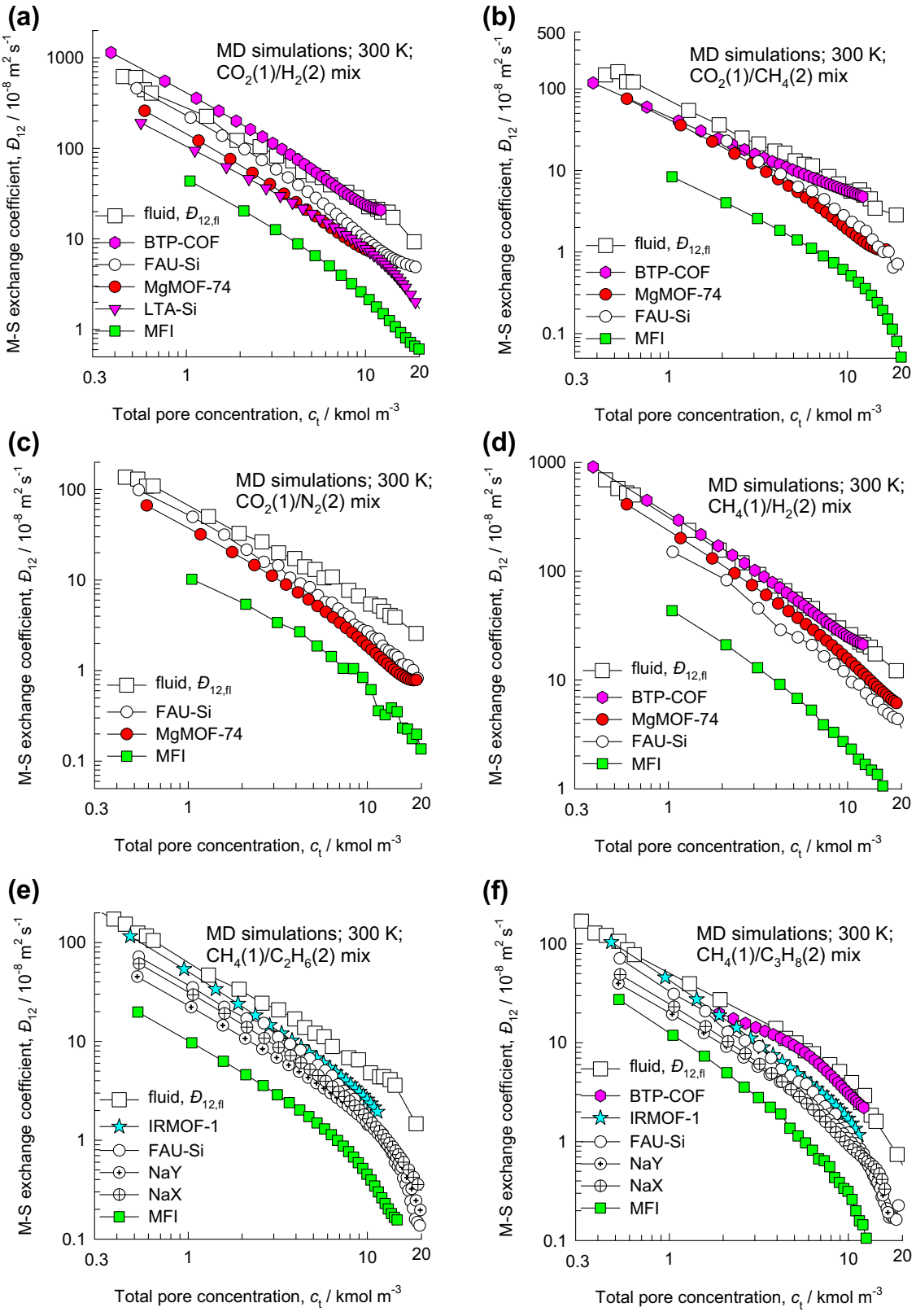

Fig. 3. The Maxwell–Stefan exchange coefficients $Đ_{12}$, for diffusion of equimolar ($c_1 = c_2$) (a) CO_2/H_2, (b) CO_2/CH_4, (c) CO_2/N_2, (d) CH_4/H_2, (e) CH_4/C_2H_6, and (f) CH_4/C_3H_8 mixtures at 300 K in a variety of host materials, as a function of the total concentration, c_t. The $Đ_{12,fl}$ for binary *fluid phase* mixture diffusion, obtained from independent MD simulations, are also presented in square symbols. The data presented included MD simulations of binary mixture diffusion in FAU-Si, NaY, NaX, IRMOF-1, and MOF-177, and details of these structures are available in Supplementary material accompanying this publication.

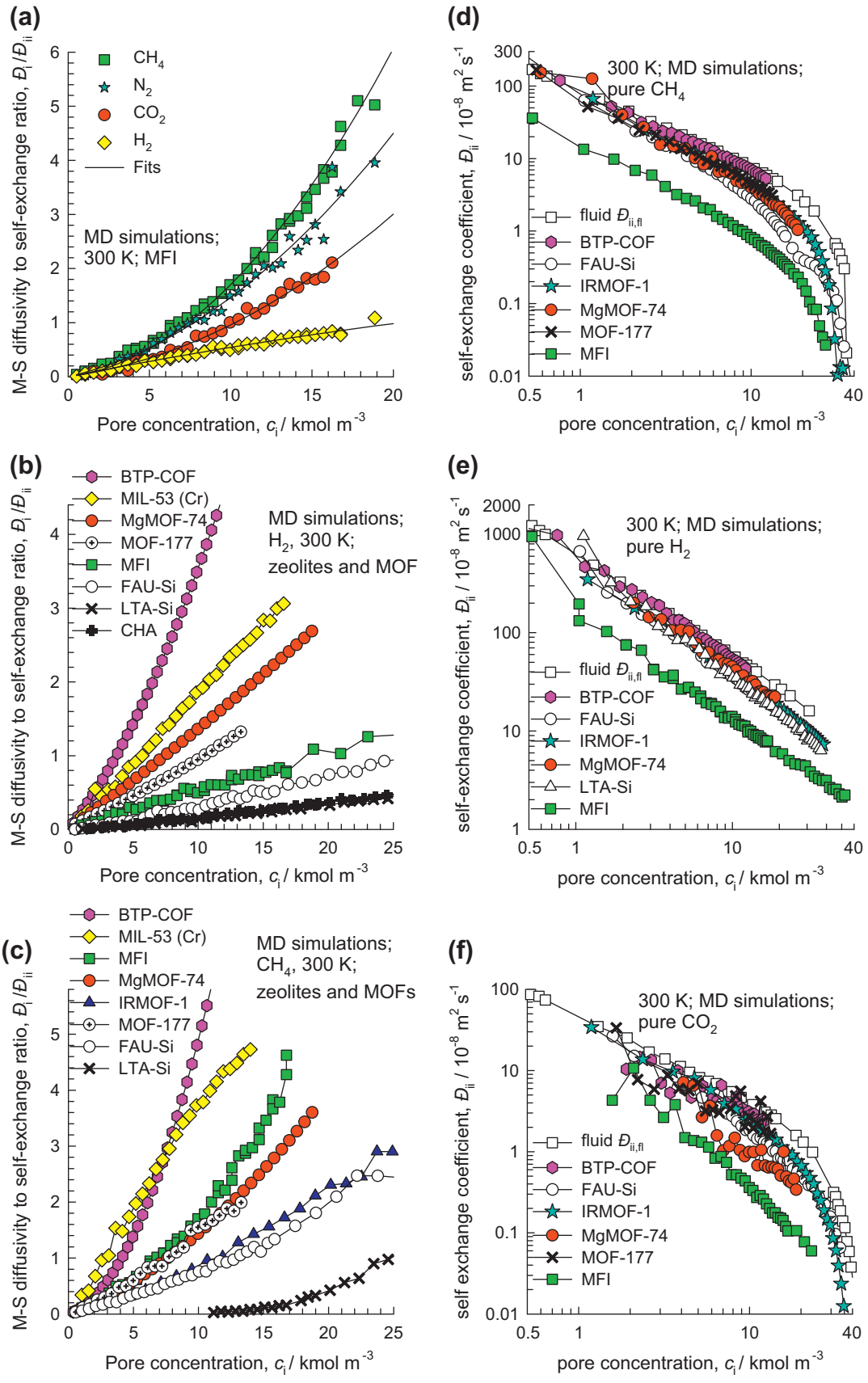

Fig. 4. The degree of correlations, $Đ_i/Đ_{ii}$, for diffusion of (a) CH_4, CO_2, N_2, and H_2 in MFI zeolite, (b) H_2, and (c) CH_4 in a variety of porous host materials. Similar data on the degree of correlations for other guest/host combinations are available in Supplementary material. The exchange coefficients, $Đ_{ii}$, for diffusion of (d) CH_4, (e) H_2, and (f) CO_2 in a variety of host materials.

the 5.5 Å channels of MFI zeolite, the $Đ_{12}$ is about a tenth of the value for the corresponding fluid mixture, when compared at the total molar concentration c_t within the pores, i.e. $F \approx 0.1$. Within the 1D, 10.4 Å sized hexagonal-shaped channels of MgMOF-74, the degree of confinement of the guest molecules is lower, and the value of $F \approx 0.7$. For FAU-Si, NaY, and NaX that has 7.4 Å sized windows separating 11 Å sized cages, the values of F are in the range 0.4–0.7. Procedures for estimation of the $Đ_{12,\mathrm{fl}}$ are available in Poling et al. [41], and therefore this provides a convenient starting point for the estimation of the $Đ_{12}$.

The link between the exchange coefficient $Đ_{12}$ with the corresponding fluid phase diffusivity $Đ_{12,\mathrm{fl}}$ is of vital importance because it paves the way for developing an interpolation formula using unary diffusion data, using the Vignes interpolation formula for liquid mixtures as a guide [42]. This approach results in the following formula [35,36]:

$$Đ_{12} = (Đ_{11})^{x_1}(Đ_{22})^{x_2} \tag{4}$$

For diffusion within porous materials, the $Đ_{ii}$ are the *self*-exchange coefficients, that are determinable from MD simulations of unary diffusion of both $Đ_i$, and the *self*-diffusivity, $D_{i,\mathrm{self}}$, by use of the following relationship:

$$\frac{1}{D_{i,\mathrm{self}}} = \frac{1}{Đ_i} + \frac{1}{Đ_{ii}} \tag{5}$$

The interpolation formula (4) has been verified on the basis of MD simulations for a wide variety of guest-host combinations [35,36]; evidence of the validation for selected guest-host combinations are available in Supplementary material accompanying this publication. The ratio $Đ_i/Đ_{ii}$ can be viewed as a measure of the degree of correlations for unary diffusion of species *i*. For any given material, $Đ_i/Đ_{ii}$ increases with increasing pore concentration. As illustration, Fig. 4a shows MD simulated data on the degree of correlations, $Đ_i/Đ_{ii}$, for diffusion of CH_4, CO_2, N_2, and H_2 in MFI zeolite. As the concentration within the pores increases, the jumps of individual molecules become increasingly correlated because the number of vacant sites will decrease, and the probability of unsuccessful jumps will increase.

The degree of correlations also depends on the pore size, connectivity and topology. Fig. 4b and c presents a comparison of $Đ_i/Đ_{ii}$ for H_2 and CH_4 diffusion in a variety of host materials. Broadly speaking, the highest degree of correlations is for 1D channel structures, such as MgMOF-74 and BTP-COF, because of the difficulty of *by-passing* of molecules. The smallest degree of correlations is realized in structures such as LTA-Si, CHA, SAPO-34, DDR, ITQ-29, and ZIF-8 that have cages separated by windows that are in the 3.4–4.1 Å size range. In such structures, the inter-cage hops across the window occur one-molecule-at-a-time and correlations are practically negligible at pore concentrations $c_t < 10$ kmol m^{-3} [6,23,43–47]. A qualitative appreciation of the molecular hops across the windows of LTA-Si, and CHA is obtained by examination of video animations available as Supplementary material accompanying this publication. For concentrations $c_t > 10$ kmol m^{-3}, intra-cage motion becomes limiting leading to sizable correlation effects.

The self-exchange coefficients $Đ_{ii}$ are relatable to the self-diffusivities in the corresponding fluid mixture, $Đ_{ii,\mathrm{fl}}$ [35,36] (see Fig. 4d–f). For mesoporous materials such as BTP-COF, $Đ_{ii} \approx Đ_{ii,\mathrm{fl}}$. For MFI zeolite, the $Đ_{ii}$ are about an order of magnitude lower than the $Đ_{ii,\mathrm{fl}}$. Engineering estimation procedures for the fluid phase self-diffusivity $Đ_{ii,\mathrm{fl}}$ are available [41], and therefore it is possible to make reasonable estimates of $Đ_{ii}$ in a given host material on the basis of the information provided in Fig. 4.

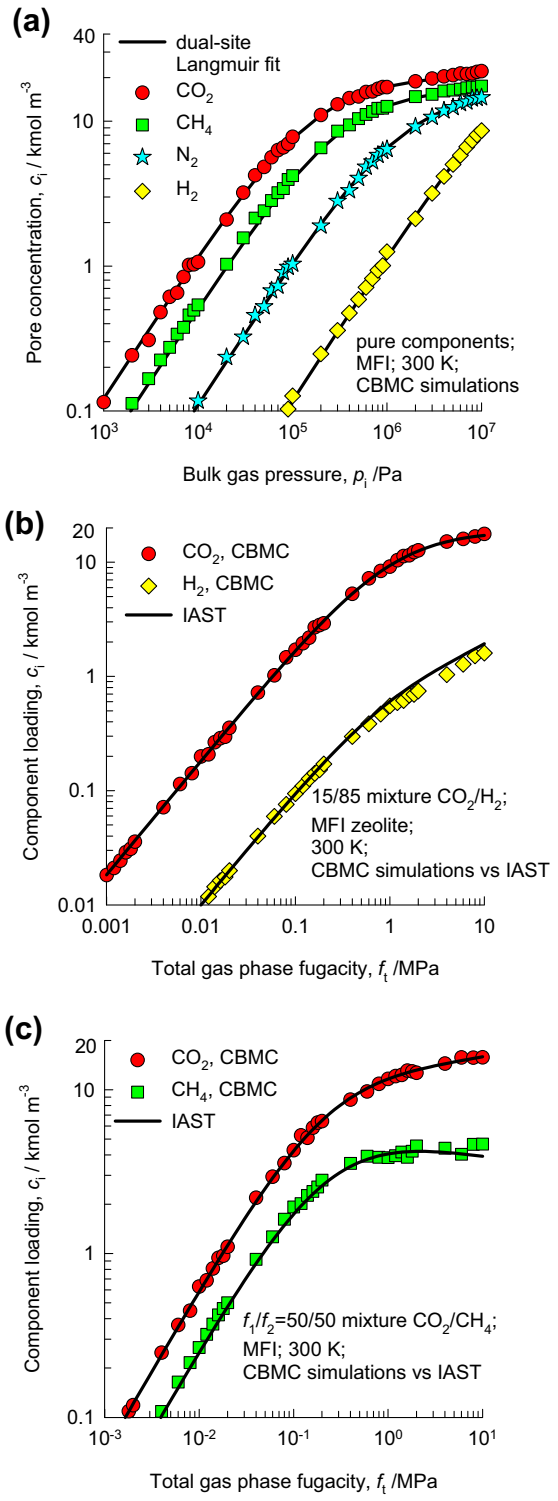

Fig. 5. (a) CBMC simulation data on the pure component adsorption isotherms of H_2, N_2, CH_4, and CO_2 in MFI at 300 K. The continuous solid lines are the dual-Langmuir–Freundlich fits of the isotherms; the fit parameters are provided in Supplementary material accompanying this publication. (b and c) CBMC simulations for component loadings in CO_2/H_2 ($p_1/p_2 = 15/85$), CO_2/CH_4 ($p_1 = p_2$), and mixtures at 300 K. The continuous solid lines are the IAST calculations using the dual-Langmuir–Freundlich fits of the CBMC simulated pure component isotherms. Similar comparisons of the IAST calculations with CBMC mixture simulations are available in Supplementary material for several other guest/host combinations.

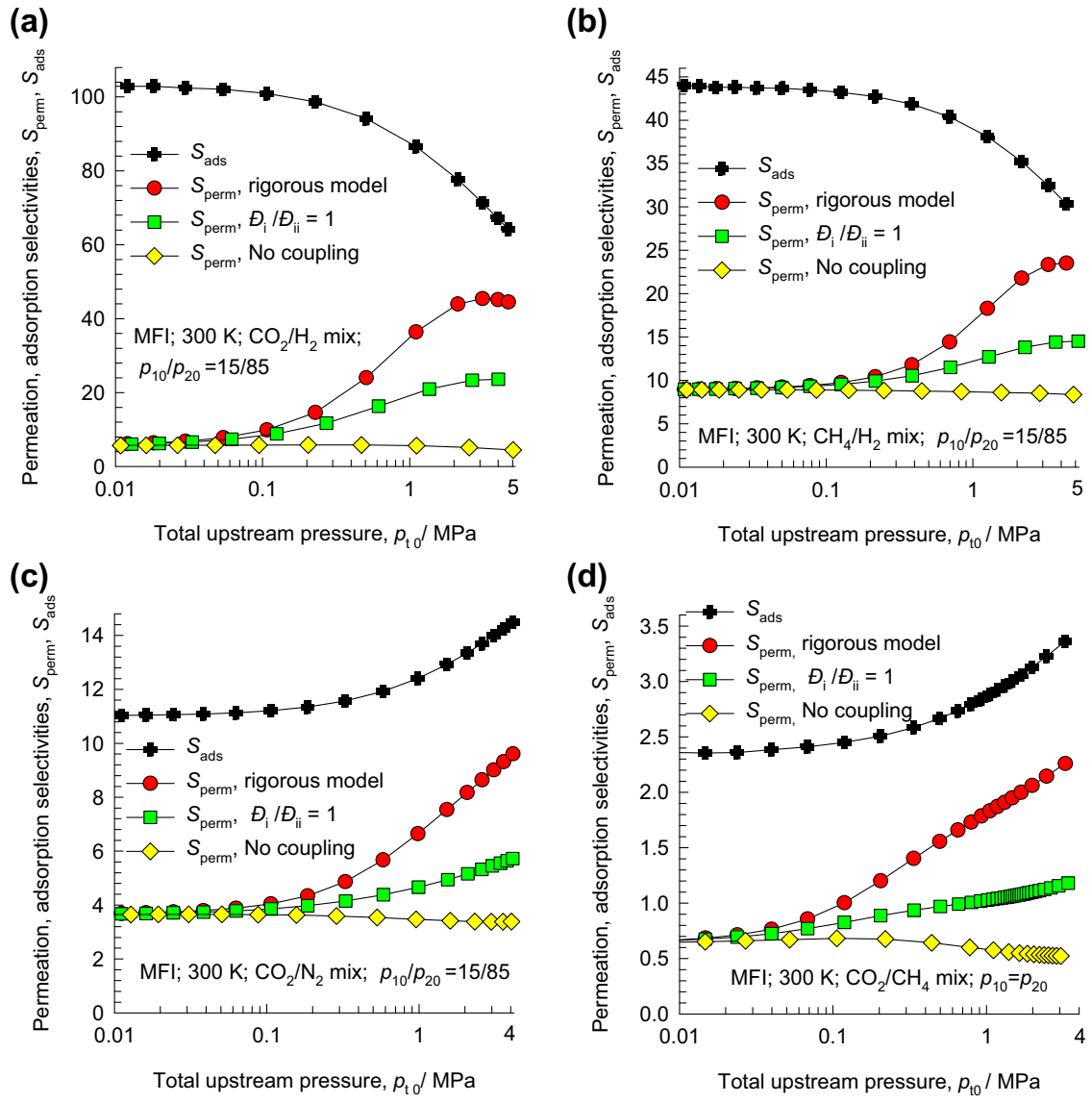

Fig. 6. The influence of different calculation procedures for the degree of correlations, $Đ_i/Đ_{ii}$, on the permeation selectivity, S_{perm}, for (a) CO_2/H_2, (b) CH_4/H_2, (c) CO_2/N_2, and (d) CO_2/CH_4 mixture permeation across an MFI membrane at 300 K, plotted as a function of the total upstream pressure, $p_{t0} = p_{10} + p_{20}$. For (a), (b) and (c) the partial pressures in the gas phase in the upstream compartment satisfy $p_{10}/p_{20} = 15/85$ along with the adsorption selectivity, S_{ads}. In (d), $p_{10} = p_{20}$. The downstream partial pressures were maintained at 10 Pa for each species in all cases. The thickness of MFI crystalline layer, $\ell = 50$ μm. The data on diffusivities, correlations, and dual-site Langmuir–Freundlich parameters for fitting of the pure component isotherms are specified in Supplementary material accompanying this publication. Video animations of the motion of mixtures of molecules across MgMOF-74, LTA-Si, and BTP-COF membranes are available as Supplementary material.

Since experimental data on the exchange coefficients are rarely available, the assumption that $Đ_i/Đ_{ii} = 1$ is often invoked [26,34,48], leading to the interpolation formula:

$$Đ_{12} = (Đ_1)^{x_1}(Đ_2)^{x_2} \tag{6}$$

We shall demonstrate later that use of Eq. (6) leads to severe underestimation of correlation effects in mixture permeation.

3. Binary mixture permeation

In order to underscore the importance of proper modeling of correlation effects we first consider permeation of (a) $CO_2(1)/H_2(2)$, (b) $CH_4(1)/H_2(2)$, (c) $CO_2(1)/CH_4(2)$, and (d) $CO_2(1)/N_2(2)$ mixtures across a MFI zeolite membrane with microporous crystalline layer of thickness $\ell = 50$ μm. For all four mixtures the species 1 has the higher adsorption strength, while the species 2 has higher mobility. A qualitative appreciation of the motion of the molecules within the intersecting channels of MFI zeolite is obtained by examination of video animations of MD simulations, available as Supplementary material accompanying this publication.

The first step is to rewrite the chemical potential gradients in Eq. (1) in a more practically usable form. The chemical potential gradients can be related to the more conventional gradients of concentrations within the pores by defining thermodynamic correction factors Γ_{ij}:

$$\frac{c_i}{RT}\frac{d\mu_i}{dz} = \sum_{j=1}^{2}\Gamma_{ij}\frac{dc_j}{dz}; \quad \Gamma_{ij} = \frac{c_i}{p_i}\frac{\partial p_i}{\partial c_j}; \quad i,j = 1,2 \tag{7}$$

For determination of the adsorbed phase pore concentrations c_i and the elements Γ_{ij}, in the binary mixtures, the Ideal Adsorbed Solution Theory (IAST) of Myers and Prausnitz [49] was used. For application of the IAST, pure component isotherm fits are required. For this purpose the dual-site Langmuir–Freundlich fits of the CBMC

simulated pure component isotherms were employed (see Fig. 5a). In order to verify the accuracy of IAST calculations, we carried out CBMC simulations for the binary mixtures. Fig. 5b and c presents comparisons of the IAST predictions with the CBMC simulation data for component loadings. We see excellent agreement of the IAST with CBMC data; this confirms the applicability of IAST for practical purposes. Similar good agreement was earlier established for adsorption of a wide variety of mixtures in different zeolites [50,51].

At steady-state, the fluxes N_i obey:

$$\frac{\partial N_i}{\partial z} = 0 \tag{8}$$

The steady state permeation fluxes N_i were determined by solving the set of Eqs. (1), (7) and (8) subject to the boundary conditions:

$$\begin{aligned} z = 0; \quad & p_i = p_{i0}; \quad c_i = c_{i0} \\ z = \ell; \quad & p_i = p_{i\ell}; \quad c_i = c_{i\ell} \end{aligned} \tag{9}$$

using the numerical procedures described in earlier works [52–54].

The M–S diffusivities $Đ_i$ were obtained from MD simulations; the concentration dependence of the $Đ_i$ follows the Reed and Ehrlich model, is described in detail in the published literature [23,36,53]. The binary exchange coefficient $Đ_{12}$, in the mixtures was estimated on the basis of the pure component self-exchange coefficients, $Đ_{ii}$, using Eq. (4) [35,45]. The data on $Đ_{ii}$ were obtained by fitting the $Đ_i/Đ_{ii}$ data plotted in Fig. 4a. All the data inputs are specified in Supplementary material accompanying this publication. For comparison purposes, we also carried out permeation calculations assuming $Đ_i/Đ_{ii} = 1$, with Eq. (6), and neglecting coupling effects, $Đ_i/Đ_{ii} \to 0$.

Fig. 6 shows the calculations of the permeation selectivity, S_{perm} defined by:

$$S_{\text{perm}} = \frac{N_1/N_2}{p_{10}/p_{20}} \tag{10}$$

where p_{i0} are the partial pressures in the upstream (feed) compartment. Also shown in Fig. 6 are IAST calculations of the adsorption selectivity, S_{ads}:

$$S_{\text{ads}} = \frac{c_{10}/c_{20}}{p_{10}/p_{20}} \tag{11}$$

where c_{i0} are the adsorption phase concentrations at the upstream face.

For CO_2/H_2, and CH_4/H_2 mixtures, S_{ads} decreases with increasing upstream feed pressure; this is due to the significantly higher saturation capacity of H_2 and the important role of entropy effects at high pressures [55]. For CO_2/N_2, and CO_2/CH_4 mixtures, S_{ads}, increases with increasing p_{t0}. It is remarkable, therefore, to note that S_{perm} is significantly increased with p_{t0} for all mixtures. This increase is directly attributable to the increase in the degree of correlations with increased loadings within the membrane. Put another way, with increased upstream feed pressure, the slowing-down effect is enhanced, resulting in a higher permeation selectivity. Correlation effects are beneficial and contribute significantly to increased values of S_{perm}. This conclusion is further underscored in the calculations of S_{perm} using the two simplified assumptions (1) $Đ_i/Đ_{ii} = 1$, and (2) $Đ_i/Đ_{ii} = 0$ (i.e. no coupling effects). The latter two simplified approaches lead to severe underestimations of S_{perm} when p_{t0} exceeds 0.5 MPa.

For CO_2/H_2 mixture permeation the component permeances, calculated from:

$$\Pi_i \equiv \frac{N_i}{p_{i0} - p_{i\ell}} \tag{12}$$

are compared in Fig. 7a with the corresponding data determination for unary permeation. For the mixture permeation calculations presented in Fig. 7a, the ratio of the partial pressures in the upstream

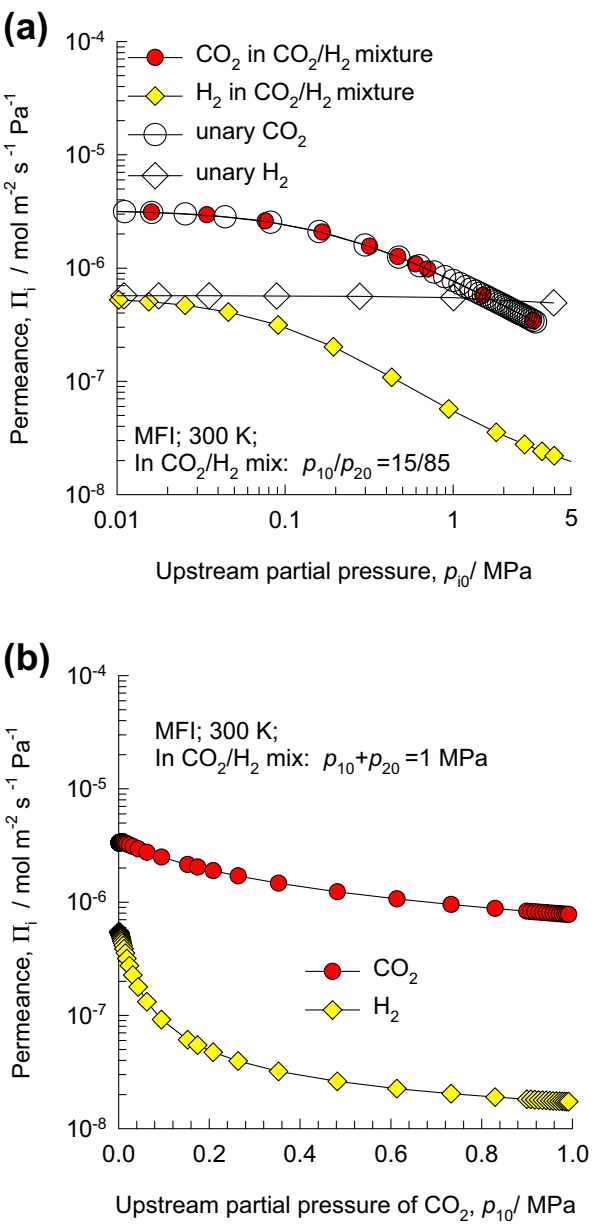

Fig. 7. (a) Influence of increase in the upstream partial pressures, p_{i0}, on the permeances of CO_2 and H_2. The data shows permeance data for unary permeation, along with permeation for $CO_2(1)/H_2(2)$ mixtures for which $p_{10}/p_{20} = 15/85$. (b) Influence of increase in the upstream partial pressure of CO_2, p_{10}, on the permeances of CO_2 and H_2 for $CO_2(1)/H_2(2)$ mixtures with a total upstream pressure held constant at $p_{t0} = p_{10} + p_{20} = 1$ MPa.

(feed) compartment were held constant $p_{10}/p_{20} = 15/85$. The trends in Fig. 7a are in close correspondence with the corresponding experimental data of Sandström et al. [16]; cf. Fig. 1a. The permeance of the tardier CO_2 in the mixture is practically the same as that for unary diffusion for the entire range of upstream (feed) partial pressures. For the more mobile H_2, the permeance in the mixture decreases by an order of magnitude below that for unary diffusion when the upstream feed pressure is increased to 5 MPa. The good agreement in the trends in Figs. 1a and 7 can be taken as an indication of the validity of the M–S formulation, and the model used for correlations. The absolute values of the permeances in Fig. 7a are about a factor 50 lower than the corresponding ones in Fig. 1a because of the significantly higher thickness of the crystalline layer assumed in our permeation calculations, 50 μm instead of the value of 0.7 μm in the Sandström experiments.

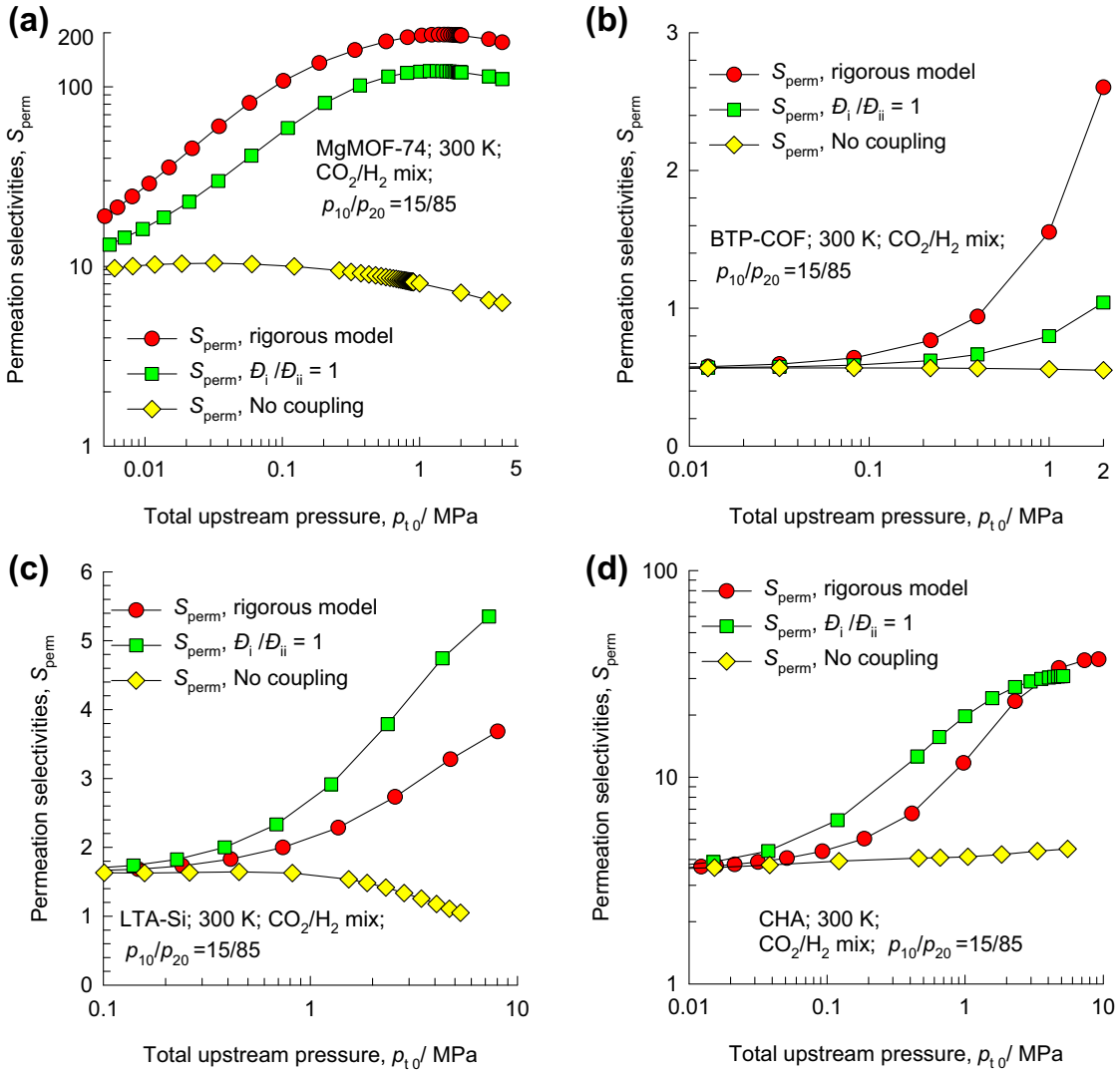

Fig. 8. The influence of different calculation procedures for the degree of correlations, $Đ_i/Đ_{ii}$, on the permeation selectivity, S_{perm}, for CO_2/H_2 mixture permeation across (a) MgMOF-74, (b) BTP-COF, (c) LTA-Si and (d) CHA membranes plotted as a function of the total upstream pressure, $p_{t0} = p_{10} + p_{20}$. The data on diffusivities, correlations, and dual-site Langmuir–Freundlich parameters for fitting of the pure component isotherms are specified in Supplementary material.

Slowing down effects on H_2 become increasingly significant when the proportion of CO_2 in the upstream (feed) compartment is increased. To demonstrate this, Fig. 7b presents calculations of the permeances of CO_2 and H_2 for $CO_2(1)/H_2(2)$ mixtures with a total upstream feed pressure held constant, $p_{10} + p_{20} = 1$ MPa. We note that the H_2 permeance decreases by more than an order of magnitude with increasing proportion of CO_2. The data presented in Fig. 7b provide a rationalization of the experimental data of David et al. [20] that show a decrease in the H_2/CO_2 selectivity with increasing proportion of CO_2 in the upstream (feed) compartment of Matrimid membranes.

For CO_2/H_2 mixture permeation across MgMOF-74, and BTP-COF membranes, the data presented in Fig. 8a and b demonstrate the importance of proper modeling of correlation effects in these materials as well. For MgMOF-74, correlation effects result in permeation selectivities that are about one order of magnitude higher than those predicted by a model that neglects coupling. The results are also dramatic for mesoporous BTP-COF; here we note that both the scenarios (1) $Đ_i/Đ_{ii} = 1$ and (2) $Đ_i/Đ_{ii} = 0$ (i.e. no coupling effects) are seen to anticipate S_{perm} values lower than unity, i.e. H_2-selective operation. In sharp contrast, the rigorous approach taking into account the increase of the degree of correlations with pore concentrations, predicts S_{perm} values greater than unity for upstream feed pressures exceeding 0.3 MPa, i.e. CO_2-selective operation.

Correlation effects in materials such as CHA, LTA, SAPO-34, DDR, and ZIF-8 are often considered to be negligible [6,17,19,22–24,46,47,56–58]. To test this assumption, we carried out CO_2/H_2 mixture permeation calculations for LTA-Si, and CHA (see Fig. 8c and d). We note the differences between the rigorous model and the scenario in which coupling is neglected are significant only when the upstream feed pressures exceed 0.5 MPa. This also rationalizes the results in Fig. 1b for permeances in SAPO-34 membrane where we note that for upstream feed partial pressures above 0.5 MPa, the H_2 permeance in the mixture is significantly lower than for the pure component.

For comparison of the CO_2/H_2 separation performance of six different materials, Fig. 9a

presents Robeson plot [59] of S_{perm} versus the CO_2 permeability defined by $\Pi_i \ell$ with total upstream feed pressure $p_{t0} = 2$ MPa. MgMOF-74 is the best of the four structures, offering both high selectivity and permeability. The high permeability of MgMOF-74 is of particular relevance to the economics of CO_2 capture, as has been emphasized by Merkel et al. [3]. A part of the success of MgMOF-74 can be traced to the high degree of correlations (cf. Fig. 4) that

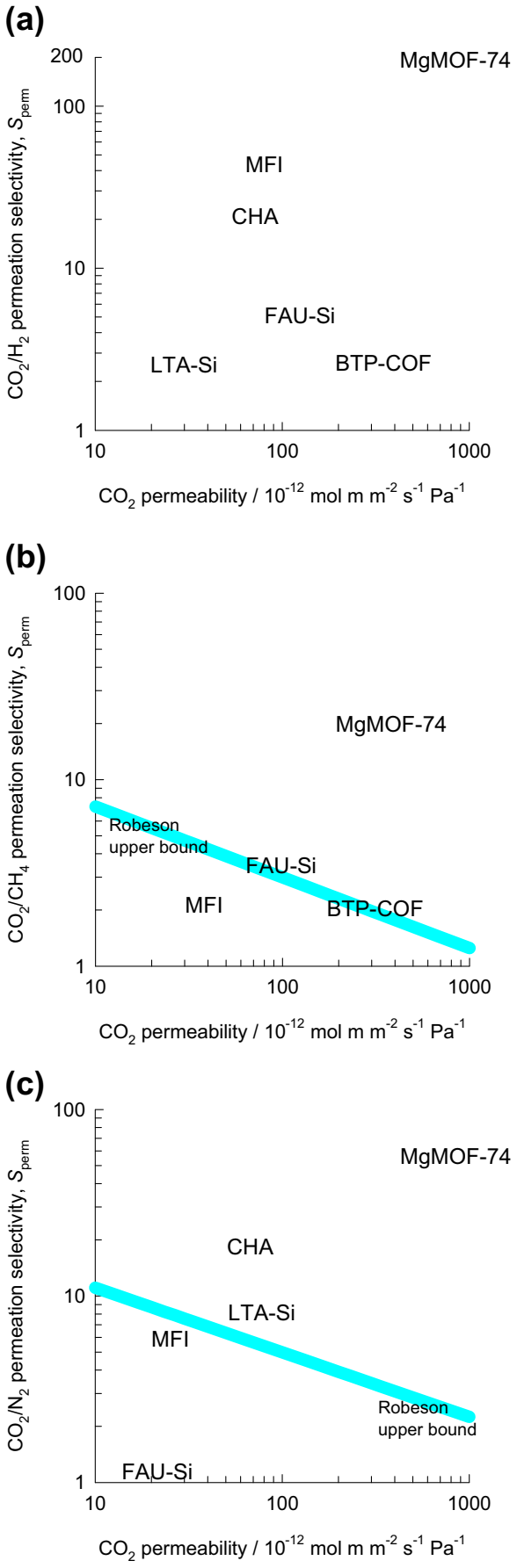

Fig. 9. Robeson plots for separation of (a) CO_2/H_2, (b) CO_2/CH_4, and (c) CO_2/N_2 mixtures, with total upstream pressure $p_{t0} = 2$ MPa, and $T = 300$ K. The permeation selectivities, S_{perm}, for different materials are plotted against the CO_2 permeability, $\Pi_i \ell$. The SI units for the permeability is mol m m^{-2} s^{-1} Pa^{-1}. The more commonly used engineering unit for permeability is the Barrer expressed in cm^3 (STP) cm cm^{-2} s^{-1} (cm Hg)$^{-1}$. To convert to the commonly used engineering units of Barrers we divide the value in mol m m^{-2} s^{-1} Pa^{-1} by 3.348×10^{-16}. Also plotted in (b and c) is the "upper bound" calculated using the parameters specified in Table 12 of Robeson [59].

enhances S_{perm}. Analogous Robeson plots for CO_2/CH_4, and CO_2/N_2 mixtures are presented in Fig. 9b and c. For these separations too, MgMOF-74 emerges as the best material with performance significantly higher than the Robeson "upper bound" [59].

4. Conclusions

Using molecular simulations of adsorption and diffusion, we have investigated the influence of correlation effects on mixture permeation across four different porous materials: MFI, LTA-Si, MgMOF-74, and BTP-COF. The following major conclusions can be drawn from this study.

(1) Coupling, or correlation, effects in binary mixture permeation are embodied in the Maxwell–Stefan formulation (1) by the exchange coefficient $Đ_{12}$.
(2) Correlation effects are strong functions of the pore concentrations, and the exchange coefficients $Đ_{12}$ decrease by about an order of magnitude with increasing pore concentrations; see Fig. 2.
(3) For mesoporous structures such as BTP-COF, the exchange coefficient $Đ_{12}$ can be identified with the corresponding fluid phase diffusivity, $Đ_{12,fl}$. For microporous structure, the exchange coefficient $Đ_{12}$ can be an order of magnitude lower than $Đ_{12,fl}$.
(4) The interpolation formula (4) provides a convenient approach for estimation of the $Đ_{12}$ for binary mixture using data on the self-exchange coefficients $Đ_{ii}$ that can be derived from unary diffusion.
(5) The degree of correlations in molecular motions, $Đ_i/Đ_{ii}$, increases as the pore concentration increases; see Fig. 4.
(6) The IAST is sufficiently accurate for estimation of binary adsorption equilibrium for mixtures, using pure component isotherm fits; see Fig. 5.
(7) The proper modeling of correlation effects, taking the concentration dependence of the $Đ_i/Đ_{ii}$ into account, is essential in the calculation of permeation fluxes and selectivities; see Figs. 6 and 8.
(8) Use of the simplified interpolation formula (6) is not recommended. This formula often under-estimates the importance of correlation effects, see Figs. 6 and 8a,b. For LTA-Si, the use of Eq. (6) over-estimates correlation effects; see Fig. 8c.
(9) The commonly made assumption that correlation effects in cage-type-structures with narrow windows (such as CHA, LTA, SAPO-34, DDR, and ZIF-8) can be considered to be negligible is likely to fail for operation at pressures exceeding about 1 MPa.
(10) The results of our study also indicate the desirability of choosing materials for CO_2 capture applications that have a high degree of correlations. In this regard, 1D channel structure of MgMOF-74 is particularly effective. The membrane performance of MgMOF-74 is anticipated to significantly exceed the Robeson "upper bound" [59].

Appendix A. Supplementary data

Supplementary data associated with this article can be found, in the online version, at doi:10.1016/j.memsci.2011.08.067.

Nomenclature

c_i	pore concentration of species i, mol m^{-3}
c_t	total concentration in mixture, mol m^{-3}
$D_{i,\text{self}}$	self-diffusivity of species i, m^2 s^{-1}
$Đ_i$	Maxwell–Stefan diffusivity, m^2 s^{-1}
$Đ_{ii}$	self exchange coefficient, m^2 s^{-1}
$Đ_{12}$	M–S exchange coefficient for binary mixture, m^2 s^{-1}
$Đ_{ij,\text{fl}}$	M–S diffusivity in binary i–j fluid mixture, m^2 s^{-1}
F	factor defined by $F \equiv Đ_{ij}/Đ_{ij,\text{fl}}$, dimensionless
ℓ	thickness of membrane, m
n	number of components in mixture, dimensionless
N_i	molar flux of species i defined in terms of the membrane area, mol m^{-2} s^{-1}
p_i	partial pressure of species i, Pa
p_{i0}	partial pressure of species i in upstream compartment (retentate), Pa
$p_{i\ell}$	partial pressure of species i in downstream compartment (permeate), Pa
p_{t0}	total system pressure in upstream compartment (retentate), Pa
R	gas constant, 8.314 J mol^{-1} K^{-1}
S_{ads}	adsorption selectivity, dimensionless
S_{perm}	permeation selectivity, dimensionless
T	temperature, K
x_i	mole fraction of species i based on loading within pore, dimensionless
z	distance along the membrane, m

Greek letters

Γ_{ij}	thermodynamic factors, dimensionless
ϕ	fractional pore volume, dimensionless
μ_i	molar chemical potential, J mol^{-1}
Π_i	permeance of species i, mol m^{-2} s^{-1} Pa^{-1}

Subscripts

0	referring to upstream face (retentate) of membrane
fl	referring to fluid phase
ℓ	referring to downstream face (permeate) of membrane
i	referring to component i
t	referring to total mixture

References

[1] J. Caro, M. Noack, Zeolite membranes—recent developments and progress, Microporous Mesoporous Mater. 115 (2008) 215–233.
[2] A.D. Ebner, J.A. Ritter, State-of-the-art adsorption and membrane separation processes for carbon dioxide production from carbon dioxide emitting industries, Sep. Sci. Technol. 44 (2009) 1273–1421.
[3] T.C. Merkel, H. Lin, X. Wei, R. Baker, Power plant post-combustion carbon dioxide capture: an opportunity for membranes, J. Membr. Sci. 359 (2010) 126–139.
[4] J. Gascon, F. Kapteijn, Metal-organic framework membranes—high potential, bright future? Angew. Chem. Int. Ed. 49 (2010) 1530–1532.
[5] E. Favre, Membrane processes and postcombustion carbon dioxide capture: challenges and prospects, Chem. Eng. J. 171 (2011) 782–793.
[6] R. Krishna, J.M. van Baten, In silico screening of zeolite membranes for CO_2 capture, J. Membr. Sci. 360 (2010) 323–333.
[7] R. Krishna, J.M. van Baten, In silico screening of metal-organic frameworks in separation applications, Phys. Chem. Chem. Phys. 13 (2011) 10593–10616.
[8] Z.R. Herm, J.A. Swisher, B. Smit, R. Krishna, J.R. Long, Metal-organic frameworks as adsorbents for hydrogen purification and pre-combustion carbon dioxide capture, J. Am. Chem. Soc. 133 (2011) 5664–5667.
[9] J.A. Mason, K. Sumida, Z.R. Herm, R. Krishna, J.R. Long, Evaluating metal-organic frameworks for post-combustion carbon dioxide capture via temperature swing adsorption, Energy Environ. Sci. 3 (2011) 3030–3040.
[10] T.M. McDonald, D.M. D'Alessandro, R. Krishna, J.R. Long, Enhanced carbon dioxide capture upon incorporation of *N,N′*-dimethylethylenediamine in the metal-organic framework CuBTTri, Chem. Sci. 2 (2011) 2022–2028.
[11] E.D. Bloch, L. Murray, W.L. Queen, S. Chavan, S.N. Maximoff, J.P. Bigi, R. Krishna, V.K. Peterson, F. Grandjean, G.J. Long, B. Smit, S. Bordiga, C.M. Brown, J.R. Long, Selective binding of O_2 over N_2 in a redox-active metal-organic framework with open iron(II) coordination sites, J. Am. Chem. Soc. 133 (2011) 14814–14822.
[12] R.D. Noble, Perspectives on mixed matrix membranes, J. Membr. Sci. 378 (2011) 393–397.
[13] R.T. Adams, J.S. Lee, T.H. Bae, J.K. Ward, J.R. Johnson, C.W. Jones, S. Nair, W.J. Koros, CO_2–CH_4 permeation in high zeolite 4A loading mixed matrix membranes, J. Membr. Sci. 367 (2011) 197–203.
[14] J.A. Sheffel, M. Tsapatsis, A semi-empirical approach for predicting the performance of mixed matrix membranes containing selective flakes, J. Membr. Sci. 326 (2009) 595–607.
[15] R.T. Adams, C. Carson, J.K. Ward, R. Tannenbaum, W.J. Koros, Metal organic framework mixed matrix membranes for gas separations, Microporous Mesoporous Mater. 131 (2010) 13–20.
[16] L. Sandström, E. Sjöberg, J. Hedlund, Very high flux MFI membrane for CO_2 separation, J. Membr. Sci. 380 (2011) 232–240.
[17] S. Li, J.L. Falconer, R.D. Noble, R. Krishna, Interpreting unary, binary and ternary mixture permeation across a SAPO-34 membrane with loading-dependent Maxwell–Stefan diffusivities, J. Phys. Chem. C 111 (2007) 5075–5082.
[18] S. Li, J.L. Falconer, R.D. Noble, R. Krishna, Modeling permeation of CO_2/CH_4, CO_2/N_2, and N_2/CH_4 mixtures across SAPO-34 membrane with the Maxwell–Stefan equations, Ind. Eng. Chem. Res. 46 (2007) 3904–3911.
[19] R. Krishna, S. Li, J.M. van Baten, J.L. Falconer, R.D. Noble, Investigation of slowing-down and speeding-up effects in binary mixture permeation across SAPO-34 and MFI membranes, Sep. Purif. Technol. 60 (2008) 230–236.
[20] O.C. David, D. Gorri, A. Urtiaga, I. Ortiz, Mixed gas separation study for the hydrogen recovery from $H_2/CO/N_2/CO_2$ post combustion mixtures using a Matrimid membrane, J. Membr. Sci. 378 (2011) 359–368.
[21] M. Yang, B.D. Crittenden, S.P. Perera, H. Moueddeb, J.A. Dalmon, The hindering effect of adsorbed components on the permeation of a non-adsorbing component through a microporous silicalite membrane: the potential barrier theory, J. Membr. Sci. 156 (1999) 1–9.
[22] R. Krishna, J.M. van Baten, Segregation effects in adsorption of CO_2 containing mixtures and their consequences for separation selectivities in cage-type zeolites, Sep. Purif. Technol. 61 (2008) 414–423.
[23] R. Krishna, J.M. van Baten, Onsager coefficients for binary mixture diffusion in nanopores, Chem. Eng. Sci. 63 (2008) 3120–3140.
[24] J. van den Bergh, W. Zhu, J. Gascon, J.A. Moulijn, F. Kapteijn, Separation and permeation characteristics of a DD3R zeolite membrane, J. Membr. Sci. 316 (2008) 35–45.
[25] J. van den Bergh, W. Zhu, J.C. Groen, F. Kapteijn, J.A. Moulijn, K. Yajima, K. Nakayama, T. Tomita, S. Yoshida, Natural gas purification with a DDR zeolite membrane; permeation modelling with Maxwell–Stefan equations, Stud. Surf. Sci. Catal. 170 (2007) 1021–1027.
[26] J.M. van de Graaf, F. Kapteijn, J.A. Moulijn, Modeling permeation of binary mixtures through zeolite membranes, AIChE J. 45 (1999) 497–511.
[27] R. Krishna, J.M. van Baten, Diffusion of hydrocarbon mixtures in MFI zeolite: influence of intersection blocking, Chem. Eng. J. 140 (2008) 614–620.
[28] J. Kuhn, J.M. Castillo-Sanchez, J. Gascon, S. Calero, D. Dubbeldam, T.J.H. Vlugt, F. Kapteijn, J. Gross, Adsorption and diffusion of water, methanol, and ethanol in all-silica DD3R: experiments and Simulation, J. Phys. Chem. C 113 (2009) 14290–14301.
[29] R. Krishna, J.M. van Baten, Hydrogen bonding effects in adsorption of water–alcohol mixtures in zeolites and the consequences for the characteristics of the Maxwell–Stefan diffusivities, Langmuir 26 (2010) 10854–10867.
[30] R. Krishna, J.M. van Baten, Mutual slowing-down effects in mixture diffusion in zeolites, J. Phys. Chem. C 114 (2010) 13154–13156.
[31] R. Krishna, J.M. van Baten, Highlighting pitfalls in the Maxwell–Stefan modeling of water–alcohol mixture permeation across pervaporation membranes, J. Membr. Sci. 360 (2010) 476–482.
[32] Y. Hasegawa, H. Hotta, K. Sato, T. Nagase, F. Mizukami, Preparation of novel chabazite (CHA)-type zeolite layer on porous α-Al_2O_3 tube using template-free solution, J. Membr. Sci. 347 (2010) 193–196.
[33] M. Yu, J.L. Falconer, R.D. Noble, R. Krishna, Modeling transient permeation of polar organic mixtures through a MFI zeolite membrane using the Maxwell–Stefan equations, J. Membr. Sci. 293 (2007) 167–173.
[34] F. Kapteijn, J.A. Moulijn, R. Krishna, The generalized Maxwell–Stefan model for diffusion in zeolites: sorbate molecules with different saturation loadings, Chem. Eng. Sci. 55 (2000) 2923–2930.
[35] R. Krishna, J.M. van Baten, Unified Maxwell–Stefan description of binary mixture diffusion in micro- and meso-porous materials, Chem. Eng. Sci. 64 (2009) 3159–3178.
[36] R. Krishna, Describing the diffusion of guest molecules inside porous structures, J. Phys. Chem. C 113 (2009) 19756–19781.

[37] R. Krishna, J.M. van Baten, Investigating the potential of MgMOF-74 membranes for CO_2 capture, J. Membr. Sci. 377 (2011) 249–260.
[38] R. Krishna, J.R. Long, Screening metal-organic frameworks by analysis of transient breakthrough of gas mixtures in a fixed bed adsorber, J. Phys. Chem. C 115 (2011) 12941–12950.
[39] R. Krishna, J.M. van Baten, Investigating the validity of the Knudsen prescription for diffusivities in a mesoporous covalent organic framework, Ind. Eng. Chem. Res. 50 (2011) 7083–7087.
[40] M. Fernandez, J. Kärger, D. Freude, A. Pampel, J.M. van Baten, R. Krishna, Mixture diffusion in zeolites studied by MAS PFG NMR and molecular simulation, Microporous Mesoporous Mater. 105 (2007) 124–131.
[41] B.E. Poling, J.M. Prausnitz, J.P. O'Connell, The Properties of Gases and Liquids, 5th edition, McGraw-Hill, New York, 2001.
[42] A. Vignes, Diffusion in binary solutions, Ind. Eng. Chem. Fundam. 5 (1966) 189–199.
[43] R. Krishna, J.M. van Baten, Influence of segregated adsorption on mixture diffusion in DDR zeolite, Chem. Phys. Lett. 446 (2007) 344–349.
[44] R. Krishna, J.M. van Baten, Insights into diffusion of gases in zeolites gained from molecular dynamics simulations, Microporous Mesoporous Mater. 109 (2008) 91–108.
[45] R. Krishna, J.M. van Baten, A simplified procedure for estimation of mixture permeances from unary permeation data, J. Membr. Sci. 367 (2011) 204–210.
[46] H. Bux, C. Chmelik, R. Krishna, J. Caro, Ethene/ethane separation by the MOF membrane ZIF-8: molecular correlation of permeation, adsorption, diffusion, J. Membr. Sci. 369 (2011) 284–289.
[47] H. Bux, C. Chmelik, J.M. Van Baten, R. Krishna, J. Caro, Novel MOF-membrane for molecular sieving predicted by IR-diffusion studies and molecular modeling, Adv. Mater. 22 (2010) 4741–4743.
[48] P.F. Lito, A.S. Santiago, S.P. Cardoso, B.R. Figueiredo, C.M. Silva, New expressions for single and binary permeation through zeolite membranes for different isotherm models, J. Membr. Sci. 367 (2011) 21–32.
[49] A.L. Myers, J.M. Prausnitz, Thermodynamics of mixed gas adsorption, AIChE J. 11 (1965) 121–130.
[50] R. Krishna, S. Calero, B. Smit, Investigation of entropy effects during sorption of mixtures of alkanes in MFI zeolite, Chem. Eng. J. 88 (2002) 81–94.
[51] R. Krishna, J.M. van Baten, Using molecular simulations for screening of zeolites for separation of CO_2/CH_4 mixtures, Chem. Eng. J. 133 (2007) 121–131.
[52] R. Krishna, R. Baur, Modelling issues in zeolite based separation processes, Sep. Purif. Technol. 33 (2003) 213–254.
[53] R. Krishna, D. Paschek, R. Baur, Modelling the occupancy dependence of diffusivities in zeolites, Microporous Mesoporous Mater. 76 (2004) 233–246.
[54] R. Krishna, R. Baur, Diffusion, Adsorption and Reaction in Zeolites: Modelling and Numerical Issues, University of Amsterdam, Amsterdam, November 11, 2003, http://www.science.uva.nl/research/cr/zeolite/.
[55] R. Krishna, B. Smit, S. Calero, Entropy effects during sorption of alkanes in zeolites, Chem. Soc. Rev. 31 (2002) 185–194.
[56] H. Bux, F. Liang, Y. Li, J. Cravillon, M. Wiebcke, J. Caro, Zeolitic imidazolate framework membrane with molecular sieving properties by microwave-assisted solvothermal synthesis, J. Am. Chem. Soc. 131 (2009) 16000–16001.
[57] Y. Li, F. Liang, H. Bux, W. Yang, J. Caro, Zeolitic imidazolate framework ZIF-7 based molecular sieve membrane for hydrogen separation, J. Membr. Sci. 354 (2010) 48–54.
[58] Y.S. Li, F.Y. Liang, H. Bux, A. Veldhoff, W.S. Yang, J. Caro, Molecular sieve membrane: supported metal-organic framework with high hydrogen selectivity, Angew. Chem. Int. Ed. 49 (2010) 548–551.
[59] L.M. Robeson, The upper bound revisited, J. Membr. Sci. 320 (2008) 390–400.